Numerical Investigation of Gas Mixing in Gas-Solid Fluidized Beds

Tingwen Li
Dept. of Chemical and Biological Engineering, University of British Columbia, 2360 East Mall, Vancouver, Canada V6T 1Z3

Yongmin Zhang
State Key Laboratory of Heavy Oil Processing, China University of Petroleum, Beijing, 102249, People's Republic of China

John R. Grace and Xiaotao Bi
Dept. of Chemical and Biological Engineering, University of British Columbia, 2360 East Mall, Vancouver, Canada V6T 1Z3

DOI 10.1002/aic.12144
Published online January 6, 2010 in Wiley Online Library (wileyonlinelibrary.com).

Gas mixing in a tall narrow fluidized bed operated in the slugging fluidization regime is simulated with the aid of computational fluid dynamics. In the first part, a parametric study is conducted to investigate the influence of various parameters on the gas mixing. Among the parameters studied, the specularity coefficient for the partial-slip solid-phase wall boundary condition had the most significant effect on gas mixing. It was found that the solid-phase wall boundary condition needs to be specified with great care when gas mixing is modeled, with free slip, partial slip and no-slip wall boundary conditions giving substantial differences in the extent of gas back mixing. Axial and radial tracer concentration profiles for different operating conditions are generally in good agreement with experimental data from the literature. Detailed analyses of tracer back mixing are carried out in the second part. Two parameters, the tracer backflow fraction and overall gas backflow fraction, in addition to axial profiles of cross-sectional averaged tracer concentrations, are evaluated for different flow conditions. Qualitative trends are consistent with reported experimental findings.
 AIChE J, 56: 2280–2296, 2010
Keywords: fluidized bed, gas mixing, back mixing, dispersion model, numerical simulation

Introduction

Gas mixing is important in gas-solid fluidized beds, playing a significant role in determining the conversion and selectivity of chemical reactions. Therefore, adequate knowledge of gas mixing behavior is needed to understand, evaluate, predict, scale-up, and optimize gas-solid fluidized bed processes.

Three coefficients are widely utilized to characterize gas mixing in fluidized beds: the axial dispersion coefficient, the radial dispersion coefficient, and the back mixing coefficient.[1] Many studies on gas mixing in different fluidization regimes have been reported.[2–11] Gas mixing is usually studied by injecting tracer gas into experimental fluidized beds.

Correspondence concerning this article should be addressed to J. R. Grace at jgrace@chbe.ubc.ca.

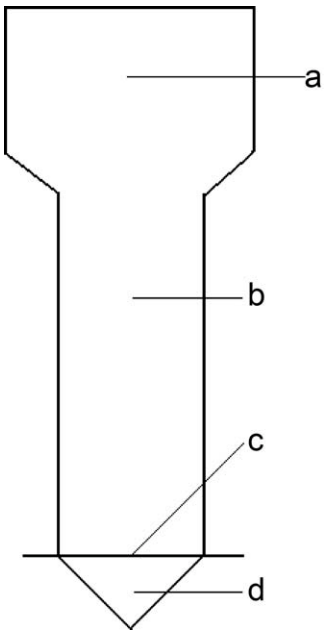

Figure 1. Schematic diagram of the apparatus of gas mixing in the experiments of Mason.[17]

(a) disengaging section, (b) fluidization column, (c) 200-mesh screen, and (d) conical windbox section).

Two modes of tracer-injection—transient and steady-state are commonly employed. Transient (pulse or step change) tracer injections, often referred to as stimulus-response methods, are normally used to obtain the residence-time distribution (RTD). This technique involves injection of a tracer into the inlet stream or at some point within the reactor and determination of the corresponding response at the exit or at some other downstream point within the reactor. For steady-state tracer studies, a tracer gas is injected continuously at a single or at several points. Samples are then taken at different positions downstream and upstream of the injection to obtain information on lateral/radial gas mixing. Regardless of the technique, the interpretation of experimental data is crucial to the correct understanding of gas mixing. Experimental data are often fitted to appropriate models to characterize the mixing characteristics of the system.[12] The most popular models are diffusion-like dispersion models and two-phase models.[7,13,14]

With the continuing improvements in computer power and numerical algorithms, computational fluid dynamics (CFD) has become a valuable tool for studying the flow in complex multiphase systems. Despite remarkable progress in CFD modeling of gas-solid fluidized beds, little numerical work on gas mixing in fluidized beds has been reported in the literature. Patil et al.[15] investigated gas dispersion and bubble-to-emulsion mass transfer in a bubbling fluidized bed based on computational and experimental studies. By introducing tracer gas from a central jet, they simulated a single rising bubble and a bubbling fluidized bed based on a two-fluid model. CFD predictions were in good agreement with experimental measurements, and fundamental insights of gas mixing with respect to bubble-to-emulsion mass exchange were obtained. Li et al.[16] carried out three-dimensional (3-D) numerical simulations of single and multiple horizontal gas jets in a small-scale rectangular bubbling fluidized bed. The mixing of secondary gas with bed materials was studied by introducing tracer into gas jets. Both transient and time-averaged results were analyzed to understand the mixing. The effect of jet velocity and jet arrangement on the mixing was also evaluated. Although good qualitative agreement was obtained with experimental and modeling results, direct quantitative comparison between numerical results and experimental data is lacking.

The objective of this study is to investigate the gas mixing in fluidized beds and the ability of CFD to predict the mixing. 3-D and 2-D numerical simulations are performed to simulate the gas mixing in a lab-scale fluidized bed operating in the slugging flow regime. Predicted axial and radial tracer concentration profiles are compared with experimental data from the literature to test the numerical predictions. Comprehensive parametric studies are next carried out to evaluate the influence of various parameters on gas mixing. Further analyses are then performed to provide insight into the gas mixing mechanisms in fluidized beds.

Experiments of Gilliland and Mason

Gilliland and Mason[2,3] carried out pioneering investigations of gas mixing in tall, narrow fluidized beds subject to steady-state tracer injection. Full details were provided by Mason.[17] In the experiments, back mixing and residence-time studies were conducted in two columns of similar geometry, but different diameter. Here, we focus our numerical simulations on the smaller unit in which the back mixing studies were conducted. The experimental column was a 76 mm I.D. cylindrical Lucite tube of height 1,830 mm, surrounded by a disengaging section of square cross section and height 914 mm, connected to a cyclone separator to recycle entrained particles. A schematic diagram of the apparatus is shown in Figure 1.

Air and two types of solid particles, spherical glass beads and petroleum cracking catalyst, were used in the experiments. For each type of bed material, particles of different sizes were used. Metered air was introduced into the bottom of the column through a conical section and was distributed by a 200-mesh screen supported by a heavier wire screen. The bed height was adjusted so that the top of the fluidized bed remained slightly below the disengaging section. To study the gas mixing, helium tracer was injected into the column through an upward-facing 5 mm glass tube on the axis of the column, 1.05 m above the distributor plate. Gas at different radial positions above and below the injection point, was then sampled through a horizontal steel tube of 1.9 mm outer diameter. In the residence-time studies, the helium was introduced into the conical section below the 200-mesh screen and sampled right above the bed surface. The tracer concentration in the gas sample were measured by a gas-density balance method and thermal conductivity analyzer. All experimental data are well tabulated.[17]

CFD model

In our numerical study, a two-fluid Eulerian-Eulerian model is employed, with each phase treated as an

Table 1. Governing Equations and Constitutive Correlations

(A) Conservation laws

Mass conservation

$$\frac{\partial}{\partial t}(\alpha_g \rho_g) + \nabla \cdot (\alpha_g \rho_g \vec{V}_g) = 0$$

$$\frac{\partial}{\partial t}(\alpha_p \rho_p) + \nabla \cdot (\alpha_p \rho_p \vec{V}_p) = 0$$

Momentum equation

$$\frac{\partial}{\partial t}(\alpha_g \rho_g \vec{V}_g) + \nabla \cdot (\alpha_g \rho_g \vec{V}_g \vec{V}_g) = \nabla \cdot \bar{\bar{\tau}}_{g,\text{eff}} - \alpha_g \nabla P + \alpha_g \rho_g \vec{g} + \beta_{gp}(\vec{V}_g - \vec{V}_p)$$

$$\frac{\partial}{\partial t}(\alpha_p \rho_p \vec{V}_p) + \nabla \cdot (\alpha_p \rho_p \vec{V}_p \vec{V}_p) = \nabla \cdot \bar{\bar{\sigma}}_p - \alpha_p \nabla P + \alpha_p \rho_p \vec{g} + \beta_{gp}(\vec{V}_p - \vec{V}_g)$$

Species transportation

$$\frac{\partial}{\partial t}(\alpha_g \rho_g Y_t) + \nabla \cdot (\alpha_g \rho_g \vec{V}_g Y_t) = \nabla \cdot \left(\left(\rho_g D_m + \frac{\mu_{g,t}}{Sc_t} \right) \nabla Y_t \right)$$

Turbulence model

$$\frac{\partial}{\partial t}(\alpha_\text{g} \rho_\text{g} k) + \nabla \cdot (\alpha_\text{g} \rho_\text{g} \vec{V}_\text{g} k) = \nabla \cdot \left(\alpha_\text{g} \frac{\mu_{\text{g},t}}{\sigma_k} \nabla k \right) + \alpha_\text{g} G - \alpha_\text{g} \rho_\text{g} \varepsilon + \Pi_{p,k}$$

$$\frac{\partial}{\partial t}(\alpha_\text{g} \rho_\text{g} \varepsilon) + \nabla \cdot (\alpha_\text{g} \rho_\text{g} \vec{V}_\text{g} \varepsilon) = \nabla \cdot \left(\alpha_\text{g} \frac{\mu_{\text{g},t}}{\sigma_\varepsilon} \nabla \varepsilon \right) + \alpha_\text{g} \frac{\varepsilon}{k}(C_1 G - C_2 \rho_\text{g} \varepsilon) + \Pi_{p,\varepsilon}$$

(B) Constitutive models Stress tensors

Stress tensors

$$\bar{\bar{\tau}}_{g,\text{eff}} = \bar{\bar{\tau}}_g + \bar{\bar{\tau}}_{g,t}$$

$$\bar{\bar{\sigma}}_p = \bar{\bar{\sigma}}_{p,vis} + \bar{\bar{\sigma}}_{p,fric}$$

Granular Kinetic Theory

$$\frac{3}{2}\left[\frac{\partial}{\partial t}(\alpha_p \rho_p \Theta_p) + \nabla \cdot (\alpha_p \rho_p \vec{V}_p \Theta_p)\right] = (-P_{s,vis}\bar{\bar{I}} + \bar{\bar{\tau}}_{p,vis}) : \vec{V}_p + \nabla \cdot \left(\kappa_{p,\Theta} \nabla \Theta_p\right) - \gamma_\Theta + \phi_{gp}$$

$$P_{s,vis} = \alpha_p \rho_p \Theta_p \, (1 + 2\alpha_p g_{0,p} \, (1 + e_p))$$

$$g_{0,p} = \frac{3}{5}\left[1 - \left(\frac{\alpha_p}{\alpha_{p,max}}\right)^{\frac{1}{3}}\right]^{-1}$$

$$\bar{\bar{\sigma}}_{p,vis} = -P_{s,vis}\bar{\bar{I}} + \bar{\bar{\tau}}_{p,vis}$$

$$\bar{\bar{\tau}}_{p,vis} = \mu_p[\nabla \vec{V}_p + (\nabla \vec{V}_p)^T] + \left(\lambda_p - \frac{2}{3}\mu_p\right)\bar{\bar{I}} \cdot \nabla \cdot \vec{V}_p$$

(*Continued*)

Table 1. (Continued)

$$\mu_p = \frac{4}{5}\alpha_p^2 \rho_p d_p g_{0,p}(1+e_p)\sqrt{\frac{\Theta_p}{\pi}} + \frac{\frac{5\sqrt{\pi}}{48}\rho_p d_p \sqrt{\Theta_p}}{(1+e_p)g_{0,p}}\left[1+\frac{4}{5}g_{0,p}\,\alpha_p(1+e_p)\right]^2$$

$$\lambda_p = \frac{4}{3}\alpha_p^2 \rho_p d_p g_{0,p}(1+e_p)\sqrt{\frac{\Theta_p}{\pi}}$$

$$\kappa_{p,\Theta} = \frac{150\rho_p d_p \sqrt{\Theta_p \pi}}{384(1+e_p)g_{0,p}}\left[1+\frac{6}{5}\alpha_p g_{0,p}(1+e_p)\right]^2 + 2\rho_p \alpha_p^2 d_p (1+e_p)\sqrt{\frac{\Theta_p}{\pi}}$$

$$\gamma_\Theta = \frac{12(1-e_p^2)g_{0,p}}{d_p\sqrt{\pi}}\rho_p \alpha_p^2 \Theta_p^{\frac{3}{2}}$$

$$\phi_{gp} = -3\beta_{gp}\,\Theta_p$$

Frictional model

$$\overline{\overline{\sigma}}_{p,fric} = -P_{s,fric}\left(\overline{\overline{I}} - \frac{\sin\phi}{\sqrt{I_{2D}}}\overline{\overline{D}}_p\right)$$

$$P_{s,fric} = \begin{cases} 0 & \alpha_p < \alpha_{p,\min} \\ Fr\frac{(\alpha_p - \alpha_{p,\min})^n}{(\alpha_{p,\max} - \alpha_p)^p} & \alpha_p \geq \alpha_{p,\min} \end{cases}$$

$Fr = 0.05;\ n = 2;\ p = 3$

Turbulence model

$$\Pi_{p,k} = \beta_{gp}\left(k_{gp} - 2k + (\vec{V}_p - \vec{V}_g)\cdot\vec{v}_{p,dr}\right)$$

$$\Pi_{p,\varepsilon} = C_3\frac{\varepsilon}{k}\Pi_{p,k}$$

$$\mu_{g,t} = \rho_g C_\mu \frac{k^2}{\varepsilon}$$

$$G = \overline{\overline{\tau}}_{g,t} : \nabla\vec{V}_g$$

$\sigma_k = 1.0;\ \sigma_\varepsilon = 1.3;\ C_1 = 1.44;\ C_2 = 1.92;\ C_3 = 1.2;\ C_\mu = 0.09$

Drag correlation

$$\beta_{gp} = \begin{cases} 150\frac{\alpha_p(1-\alpha_g)\mu_g}{\alpha_g d_p^2} + 1.75\frac{\alpha_p\rho_g|\vec{V}_p - \vec{V}_g|}{d_p} & \text{if } \alpha_g < 0.8 \\ \frac{3}{4}C_{D,p}\alpha_g^{-2.65}\frac{\alpha_p\alpha_g\rho_g|\vec{V}_p - \vec{V}_g|}{d_p} & \text{if } \alpha_g \geq 0.8 \end{cases}$$

$$C_{D,p} = \begin{cases} \frac{24}{\mathrm{Re}_p\cdot\alpha_g}(1+0.15(\mathrm{Re}_p\cdot\alpha_g)^{0.687}) & \text{if } \mathrm{Re}_p\cdot\alpha_g < 1000 \\ 0.44 & \text{if } \mathrm{Re}_p\cdot\alpha_g \geq 1000 \end{cases}$$

$$\mathrm{Re}_p = \frac{\rho_g|\vec{V}_p - \vec{V}_g|d_p}{\mu_g}$$

interpenetrating continuum. Mass and momentum conservation equations are solved for the gas and solid (particulate) phases, with appropriate closure relations. The flow is assumed to be isothermal and the gas phase incompressible. Governing equations for the solid phase are closed by granular kinetic theory.[18,19] The $k - \varepsilon$ model is employed to

Table 2. Material Properties and Base Operating Conditions

Property	Value
Particle diameter, d_p	155 μm
Particle density, ρ_p	2420 kg/m^3
Superficial gas velocity, U_g	0.183, 0.274, and 0.354 m/s
Expanded bed height, H	1.8 m
Gas density, ρ_g	1.2 kg/m^3
Gas viscosity, μ_g	1.8×10^{-5} Pa.s
Diffusion coefficient, D_m	2.88×10^{-5} m^2/s
Schmidt number, Sc	0.52
Restitution coefficient, e_p	0.98
Specularity coefficient, ϕ	0.05
Particle-wall restitution coefficient, e_w	0.8

model the gas-phase turbulence, with additional terms to take into account the effect of dispersed solid phase. The conservation equations of mass and momentum for each phase and constitutive relations, summarized in Table 1, are solved using Fluent 6.3 software.[20]

In Table 1, subscripts g and p denote the gas and particulate phases, respectively; α, ρ are the volume fraction and density; d is the diameter, and $\vec{V}$ velocity. P is the gas pressure shared by both phases; β represents the interphase drag coefficient; and $\vec{g}$ is the gravitational acceleration. D_m is the molecular diffusivity; $\mu_{g,t}$ the turbulent viscosity and Sc_t the turbulent Schmidt number. Θ is the granular temperature, P_s the solid pressure, e_p the restitution coefficient for interparticle collisions, and $\alpha_{p,\max}$ the maximum volume fraction occupied by particles.

The numerical domain matched the experimental setup, except for the disengaging section where a round cross section is simulated. The cylindrical column was discretized with about 0.1 million grid points. The mean grid size is about 4 mm, slightly coarser in the disengaging section. The grid size for a grid-independent simulation is mainly determined by the particle size.[21] Given previous simulations of gas-solid fluidized bed of similar particles,[22,23] the current grid size is believed to be sufficient. In addition, a grid-independent study was performed for 2-D simulations with grid sizes of 3, 4, and 5 mm. No significant differences were observed for all of these grids. A 3-D grid-independent study could not be performed due to the extremely high-computational load of the 3-D simulation, with a typical computational time of 8 h for 1 s of real-time simulation on a workstation with two quad-core Intel Xeon CPUs working at 2.93 GHz.

The particle (glass beads) properties and operating conditions are listed in Table 2, whenever possible obtained from the literature.[17] When parameters were not reported, such as static bed height, restitution coefficients and specularity coefficient, reasonable values were assumed based on previous work in the literature. Parametric studies were later performed on these parameters as discussed below.

At the lateral sidewall, we adopted a no-slip boundary condition for the gas phase and a partial-slip boundary condition for the solid phase[24]

$$\vec{n} \cdot \mu_p \nabla \vec{V}_{p,w} = -\frac{\pi \phi \rho_p \alpha_p \vec{V}_{p,w} g_{0,p} \sqrt{3\Theta_p}}{6\alpha_{p,\max}} \quad (1)$$

and

$$\vec{n} \cdot \kappa_{p,\Theta} \nabla \Theta_p = \frac{\pi}{6}\sqrt{3}\frac{\alpha_p}{\alpha_{p,\max}}\rho_p g_{0,p}\sqrt{\Theta_p}V_{p,w}^2 - \frac{\pi}{4}\sqrt{3}\frac{\alpha_p}{\alpha_{p,\max}}(1-e_w^2)\rho_p g_{0,p}\Theta_p^{\frac{3}{2}} \quad (2)$$

Here $\vec{n}$ is the unit vector normal to the wall, and $\vec{V}_{p,w}$ the particle slip velocity parallel to the wall. ϕ is the specularity coefficient, an empirical parameter qualifying the nature of particle-wall collisions. Its value depends on the roughness of the wall and ranges from zero for perfect specular collisions to unity for perfectly diffuse collisions. A smaller specularity coefficient generally denotes a smooth wall with less friction. In Eq. 2, e_w is the particle-wall restitution coefficient, and $\kappa_{p,\Theta}$ is the diffusion coefficient for granular energy. At the top boundary, constant pressure was assumed, and particles were free to leave the system. For the bottom distributor and the tracer flow inlet, uniform gas velocities were specified, with no particles entering the domain.

In the simulations, the bed was initially charged with stationary particles to a certain height with a volume fraction of 0.6. The particles were then fluidized by the primary gas flow through the bottom distributor. After fully developed flow was achieved, helium was continuously injected into the system through the central tube 1.05 m above the distributor.

Results and Discussion

In this section, numerical results are presented and compared with the experimental data. The influence of several parameters, including bed height, tracer flow rate, restitution coefficient, turbulence diffusion, and wall boundary condition, on the tracer back mixing is then analyzed. Finally, gas back mixing is investigated in terms of two new parameters—tracer backflow fraction and gas backflow fraction.

General flow behavior

According to the Stewart and Davidson correlation,[25] the minimum slugging velocity for a deep cylindrical column can be estimated by

$$U_{ms} = U_{mf} + 0.07\sqrt{gD} \quad (3)$$

where D is the column diameter, and U_{mf} is the minimum fluidization velocity, which can be estimated by the Wen and Yu correlation.[26] In this study, three different superficial gas velocities, 0.183, 0.274, and 0.354 m/s, were simulated, all well above the minimum slugging velocity of 0.08 m/s predicted by Eq. 3. In a recent experimental study on the transition from bubbling to turbulent fluidization in a column of 0.07 m dia. with very similar material properties,[27] the transition velocity for 159 μm glass beads from slugging to turbulent fluidization was reported to be 0.9 m/s. Hence, it is expected that all three cases are in the slugging regime. Our simulations also predicted slugging flow patterns.

Tracer concentration profiles

When helium was injected upward through the central tube at a constant flow rate, the mean concentrations in the exit stream were found to be ~16%, 16%, and 11% for

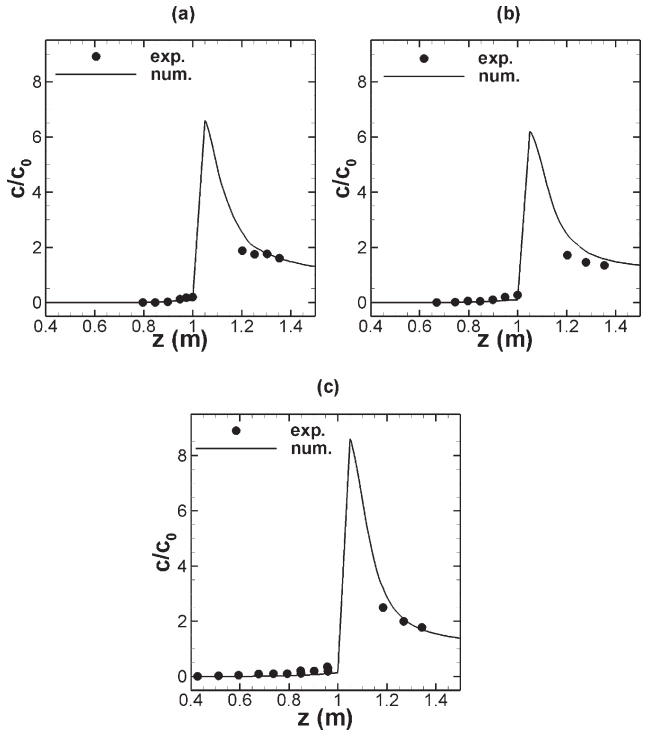

Figure 2. Axial profiles of specific tracer concentration at $r = 0$ for U_g = (a) 0.183 m/s, (b) 0.274 m/s, and (c) 0.354 m/s.

superficial gas velocities of 0.183, 0.274, and 0.354 m/s, similar to the corresponding experimental mole fractions of 16.5%, 16.5% and 9.2%. As in the experimental gas sampling, transient numerical results were averaged over 20 s intervals to obtain steady tracer concentration profiles. The first 15 s after initiating tracer injection is excluded to eliminate startup effects. Tracer concentrations are usually scaled with the exit tracer concentration c_0, defined as

$$c_0 = Q_{\text{tracer}}/Q_{\text{gas}} \tag{4}$$

where Q_{tracer} is the volumetric flow rate of tracer at the injector and Q_{gas} is the total gas flow rate at the exit.

Axial concentration profiles

Axial profiles of specific tracer concentrations at the central axis ($r = 0$) are compared with experimental data from the literature in Figure 2 for three superficial gas velocities.[17] There are no data on the axis from 1.0 to 1.05 m due to the presence of the tracer injection tube. As for the experimental measurements, the concentration is very high immediately above the injection point, decreasing gradually downstream due to radial dispersion. Low tracer concentrations are predicted below the injection level, indicating finite back mixing.

Similar axial profiles of the specific concentration at $r =$ 28 and 36 mm are compared with experimental data in Figures 3 and 4, respectively. The simulated results again show a trend similar to the experimental data.

The experimental steady tracer concentration distribution is assumed to be axisymmetric. To test this assumption, axial profiles of mean tracer concentrations are compared for azimuthal angles of 0, 90, 180, and 270° in Figure 5. Good consistency among them confirms good axisymmetry in the time-averaged flow field.

Radial profiles

Radial profiles of tracer concentration at several downstream levels are compared with experimental data in Figure 6. Again, the experimental data were measured along one radius. Both predicted and experimental profiles are bell shaped, with the maxima directly above the injection point. Numerical predictions show good agreement with the experimental data, except for over-prediction of the concentration peaks at a height of 1.2 m. This may be due to limited grid resolution at the tracer injection port. Moreover, experimental measurement of tracer concentration immediately downstream of the injection is very difficult, leading to high uncertainty in these data points relative to others.[17]

Upstream tracer is the major concern in gas back mixing studies. Numerical radial concentration profiles at different upstream levels are compared with experimental data in Figure 7. There is good qualitative agreement, with substantial gas back mixing close to the wall. However, the magnitude of specific tracer concentration is underpredicted by about 60%, except for $U_g = 0.183$ m/s at z = 0.8 and 0.9 m. This underprediction is more significant for high-superficial gas velocities, as discussed in the next section.

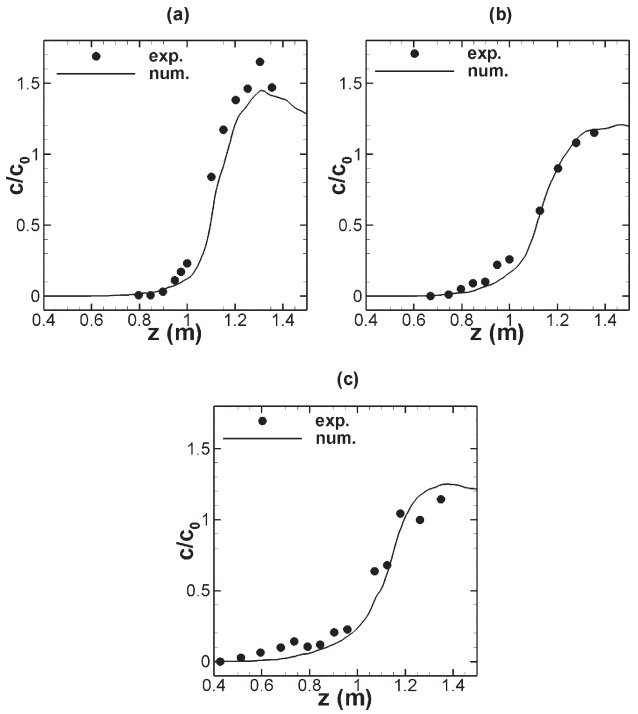

Figure 3. Axial profiles of specific tracer concentration at $r = 28$ mm for U_g = (a) 0.183 m/s, (b) 0.274 m/s, and (c) 0.354 m/s.

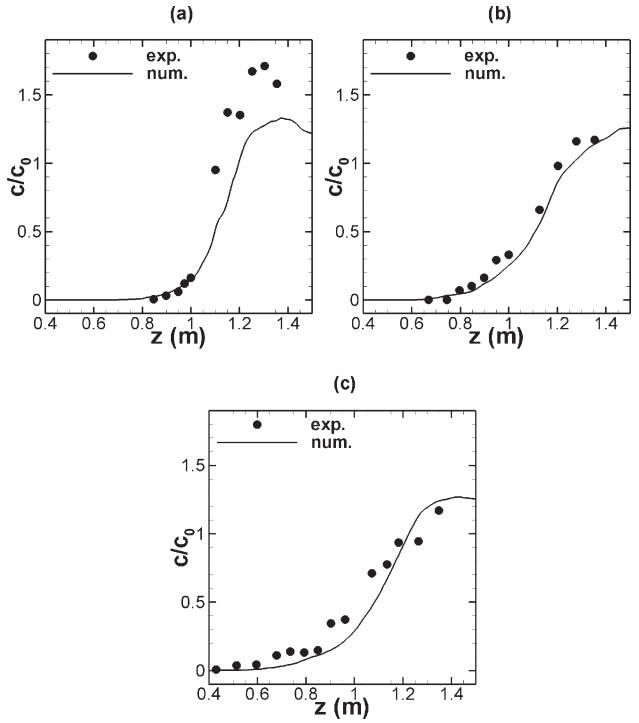

Figure 4. Axial profiles of specific tracer concentration at r = 36 mm for U_g = (a) 0.183 m/s, (b) 0.274 m/s, and (c) 0.354 m/s.

Parametric studies

In numerical simulations, parametric study is needed when the exact value of an input parameter is not available or when the sensitivity of results to a certain parameter is required. In the experiments,[2] values of the static bed height, tracer gas flow rate, and restitution coefficients were not reported. In the aforementioned simulations, values for these parameters were approximate. Here, parametric studies are undertaken to investigate the impact of these parameters on the simulation results, in particular, on the gas mixing behavior, and to identify the reason for under-predicting the back mixing. In addition, the applicability of some modeling assumptions is examined.

Even with greatly improved computational facilities, 3-D simulations are expensive and time-consuming. Hence, 2-D simulations are often performed to study hydrodynamics in 3-D columns.[28–33] However, there are hydrodynamic differences between 2-D and 3-D fluidized beds.[34] Differences between 2-D and 3-D numerical simulations of fluidized beds have been discussed,[35–37] and the reasons for the differences have been analyzed.[38] Caution must be taken when using 2-D numerical simulations to predict 3-D behavior in slugging and turbulent fluidized beds. However, 2-D simulations can be used to conduct sensitivity analyses. Here, 2-D simulations are carried out for the system, represented by an axial slice at the center of the column. Except where otherwise noted, values in Table 2 are used for the parametric studies.

Comparison between 2-D and 3-D results

Before performing the sensitivity analyses, differences between the 2-D and 3-D simulations were briefly examined by comparing radial profiles of voidage, gas and solid velocities, and tracer concentration. The tracer flow rate in the 2-D simulation was set to match c_0 in the 3-D simulation. All other conditions were the same. To eliminate the influence of the central tracer injection, only upstream profiles are compared. Figure 8 compares profiles of mean solid-volume fraction, gas and solid vertical velocities, and tracer concentration at z = 0.9 m for 2-D and 3-D simulations. There are significant differences between the 2-D and 3-D

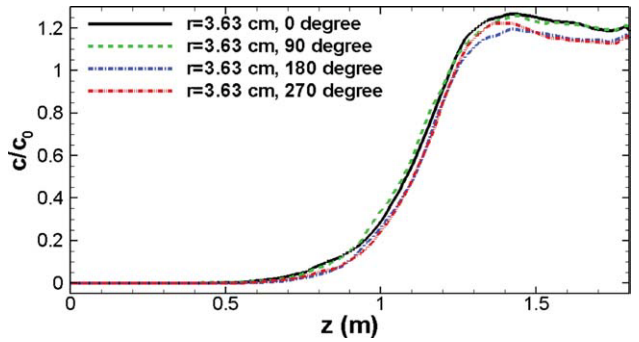

Figure 5. Axial profiles of mean tracer concentration at r = 3.63 cm at different azimuthal angles for U_g = 0.354 m/s.

[Color figure can be viewed in the online issue, which is available at wileyonlinelibrary.com.]

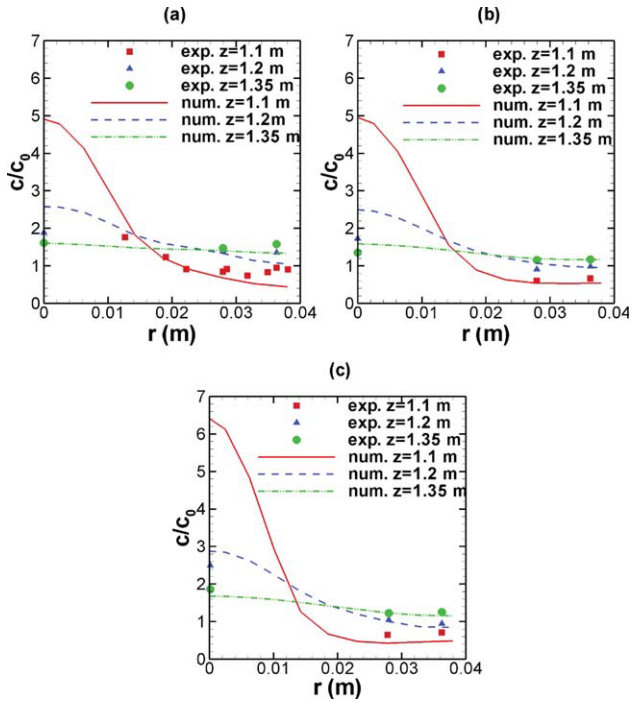

Figure 6. Radial profiles of mean tracer concentration at downstream levels for U_g = (a) 0.183 m/s, (b) 0.274 m/s, and (c) 0.354 m/s.

[Color figure can be viewed in the online issue, which is available at wileyonlinelibrary.com.]

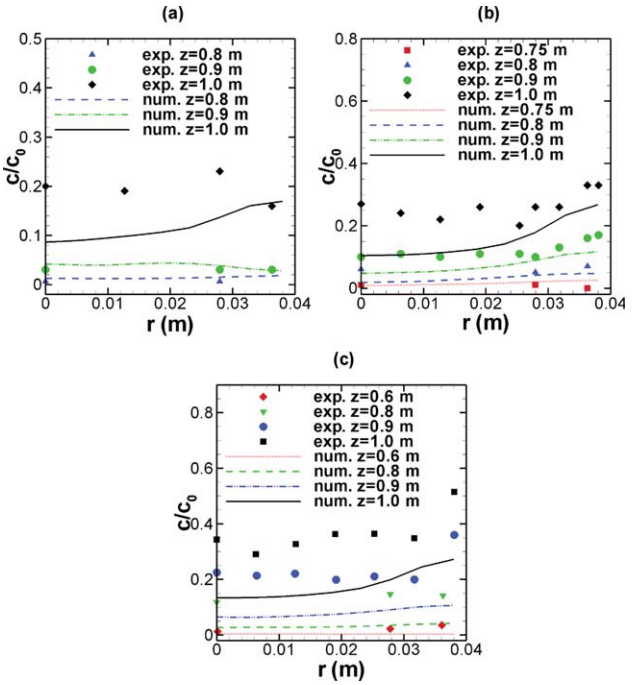

Figure 7. Radial profiles of mean tracer concentration at upstream levels for U_g = (a) 0.183 m/s, (b) 0.274 m/s, and (c) 0.354 m/s.

[Color figure can be viewed in the online issue, which is available at wileyonlinelibrary.com.]

simulations, although they are qualitatively similar. These results emphasize that 2-D simulations can only be used to perform qualitative sensitivity analyses, a finding consistent with results in the literature.[37]

Bed height

The static bed height influences the hydrodynamics and chemical reaction in fluidized-bed reactors. In the experiments, the mass of particles in the bed for any given superficial gas velocity was adjusted so that few particles entered the bottom of the disengaging section.[3] Hence, the expanded bed heights were maintained at ~1.8 m in our simulation. To investigate the influence of static bed height on gas back mixing, three initial bed heights of 0.92, 0.81, and 0.73 m were simulated, with an initial solid-volume fraction of 0.6. The corresponding expanded bed heights are about 1.85, 1.65, and 1.45 m for $U_g = 0.35$ m/s. As for the 3-D results, the mean concentration was obtained by averaging the transient results for 20 s. It was noted that the 2-D concentration profiles tend to show less symmetry than the 3-D simulations. Gas back mixing was slightly higher for the high-bed loadings, but the impact of bed height was small. For example, the mean difference between tracer concentrations at $z = 1.0$ m are 6% for bed heights of 1.65 and 1.85 m and 17% for bed heights of 1.45 and 1.85 m.

Tracer flow rate

In the experiments, tracer was injected at flow rates such that the mean concentration in the exit stream was ~10% in most runs. However, for low-superficial gas velocities, c_0 was as high as 16%.[17] In our simulations presented above, c_0 was 11 and 16% for high- and low-superficial gas velocities, respectively. Here, c_0 of 11 and 16% are simulated for $U_g = 0.35$ m/s. Tracer concentration profiles at three upstream levels z = 0.7, 0.9, and 1.0 m are plotted in Figure 9. It can be seen that tracer back mixing was higher for low-tracer flow rates than for high-tracer flow rates. This is attributable to the increased upward gas velocity through the tracer inlet as the tracer flow rate increased, causing the tracer to penetrate further downstream, making it more difficult to be carried upstream by downward solids flow. In our 3-D simulations, the differences between the numerical and experimental tracer flow rates were too small for this to explain the significant CFD underprediction of upstream concentration.

Particle-particle restitution coefficient

The particle-particle restitution coefficient is an important parameter in granular kinetic theory, characterizing the energy dissipation due to inelastic collisions. For glass beads of 3 mm in diameter, the restitution coefficient measured in detailed impact measurements at room-temperature is about 0.97 ± 0.01.[39] However; the restitution coefficient is not truly constant. Instead it depends on the impact velocity, and is said to approach unity when the impact velocity approaches zero.[40] In numerical simulations, this parameter is treated as a constant and usually set in the range 0.9–0.995.[31,41–47] Although the influence of restitution coefficient has often been studied, it was still deemed to be necessary to perform a sensitivity analysis for this parameter as no

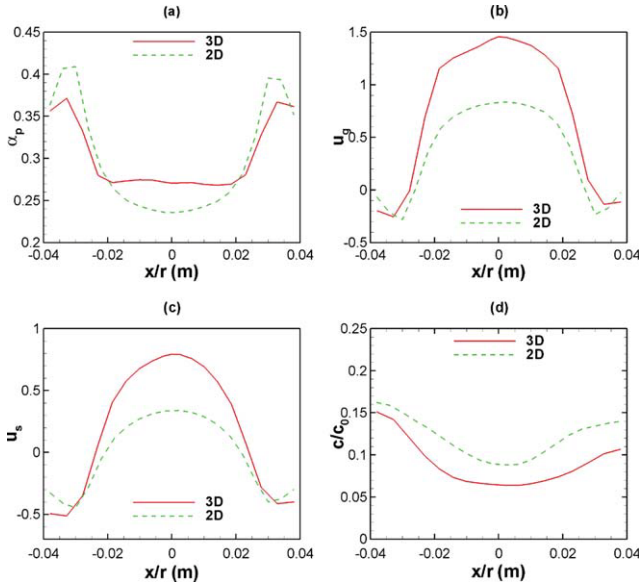

Figure 8. Radial profiles of time-averaged (a) solid-volume fraction, (b) gas-vertical velocity, (c) solid-vertical velocity, and (d) tracer concentration at z = 0.9 m from 2-D and 3-D simulations (U_g = 0.35 m/s, H_0 = 0.92 m, c_0 = 0.11, e_p = 0.98, ϕ = 0.05, e_w = 0.8).

[Color figure can be viewed in the online issue, which is available at wileyonlinelibrary.com.]

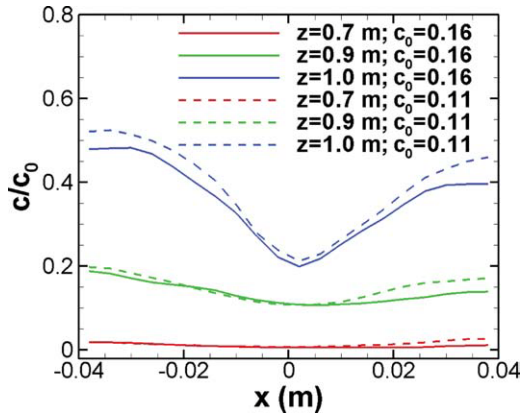

Figure 9. Influence of tracer flow rates on lateral profiles of tracer concentration at different upstream levels (U_g =0.35 m/s, H_0 = 0.92 m, e_p = 0.98, no-slip wall, e_w = 0.8).

[Color figure can be viewed in the online issue, which is available at wileyonlinelibrary.com.]

information has been reported on its influence on gas mixing. e_p = 0.9, 0.95, and 0.98 were tested. It has been reported in the literature that lower restitution coefficients lead to increased void fraction gradients and larger bubbles.[42,46] In our study, the choice of restitution coefficient was found to have minimal influence on gas mixing for the range investigated.

Turbulence diffusivity

In two-phase flows, the turbulence of the carrier phase (continuous phase) plays an important role in mixing. Considerable work has been done to model gas-phase turbulence by taking interfacial turbulent momentum transfer into account. However, a generally applicable turbulence model for two-phase flow is not available. For dense solid flows dominated by particle-particle collisions, such as flows in bubbling or slugging fluidized beds, the turbulence of the carrier phase is not of primary concern, and ignoring the gas-phase turbulence may be a practical approximation. It has been reported that gas turbulence has a negligible effect on solids flow, as the inertia of particles damps out the turbulence in the carrier phase.[48–51] For most numerical simulations of bubbling fluidized beds, no turbulence model or only a simple subscale-grid model is used for the gas phase. In this study, a dispersed turbulence model is employed to model the gas flow with dilute suspension.[20] When considering the fact that turbulent diffusion usually overwhelms molecular diffusion in most flow problems, it is interesting to examine the effect of turbulence on gas back mixing.

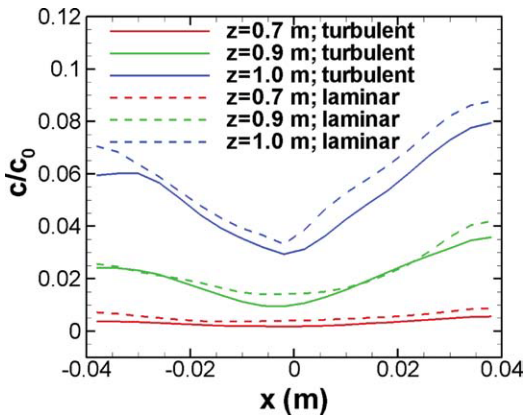

Figure 10. Influence of turbulence on lateral profiles of tracer concentration at different upstream levels (U_g = 0.35 m/s, H_0 = 0.92 m, ϕ = 0.05, e_w = 0.8 , c_0 = 0.16).

[Color figure can be viewed in the online issue, which is available at wileyonlinelibrary.com.]

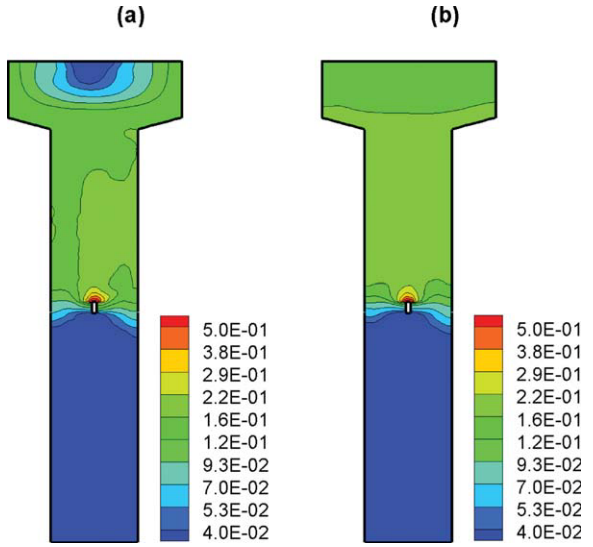

Figure 11. Contours of mean tracer concentration predicted by (a) laminar, and (b) turbulent flow assumptions (U_g = 0.35 m/s, H_0 = 0.92 m, c_0 = 0.16, ϕ = 0.05, e_w = 0.8).

[Color figure can be viewed in the online issue, which is available at wileyonlinelibrary.com.]

The influence of turbulent diffusivity is evaluated by turning on and off the turbulence model in 2-D simulations. As expected, there is no substantial difference in both mean solid-volume fraction and velocities profiles with/without the turbulence. The tracer concentration profiles at upstream levels are plotted in Figure 10 for the numerical simulations with turbulent and laminar flow assumptions. Gas turbulence is seen to have only a moderate influence on the predicted tracer back mixing since back mixing is mainly caused by solids downflow, which is almost unaffected by the gas turbulence. However, in the downstream region, differences can be observed in the tracer concentration contours as shown in Figure 11. It is evident that turbulence enhances downstream radial mixing, especially in the freeboard region, where turbulent dispersion dominates the gas mixing. In view of this finding, turbulence should clearly be considered when modeling overall gas mixing in fluidized beds.

Wall-boundary condition

No-, partial- and free-slip wall-boundary conditions for the solid phase have been used in numerical simulations of

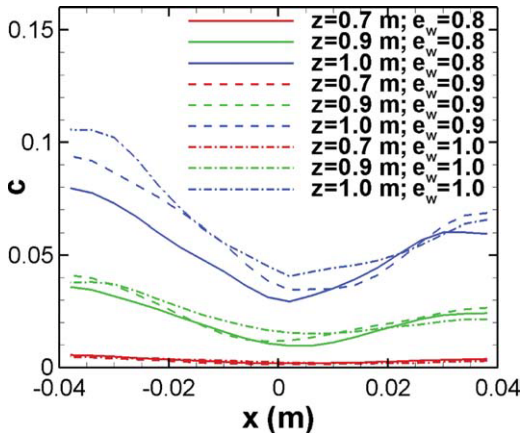

Figure 12. Effect of particle-wall restitution coefficients on lateral tracer concentration profiles at different upstream levels (U_g = 0.35 m/s, H_0 = 0.92 m, c_0 = 0.16, ϕ = 0.05).

[Color figure can be viewed in the online issue, which is available at wileyonlinelibrary.com.]

different fluidization systems. The partial-slip wall boundary condition proposed by Johnson and Jackson[24] is most widely used, requiring that, the specularity coefficient and particle-wall restitution coefficient be specified. Direct measurement of specularity coefficient is not feasible. Different values of the specularity coefficient have been used in most numerical simulations. Values of ~0.5 are most common. A low value is sometimes applied to high-velocity gas-solid flows such as circulating fluidized beds.[52–55] Benyahia et al.[54] reported that the specularity coefficient strongly affects the core-annular flow pattern in dilute gas-solid systems. Zhang and Yu[56] found a significant influence of wall boundary conditions on the hydrodynamics of slugging fluidized beds, but no work has been reported on the effect of the specularity coefficient on mixing.

The wall-particle restitution coefficient specifies the dissipation of particle granular energy by collisions with wall. No data on this parameter were reported in the experiments of Mason.[17] Here, the influence of wall-particle restitution coefficient is examined for e_w = 0.8, 0.9 and 1.0. Upstream concentration profiles are shown in Figure 12. A higher particle-wall restitution coefficient tends to increase the gas back mixing slightly. It has been reported[57,58] that the wall restitution coefficient plays only a minor role, consistent with this study where varying the wall-restitution coefficient did not affect the model predictions significantly, especially far upstream.

Predicted upstream tracer concentration profiles are compared in Figure 13 for ϕ = 0.5, 0.05, 0.005, and 0. Predictions corresponding to the no-slip solid-phase wall boundary condition are also presented. As in previous studies,[53,54] a small specularity coefficient leads to higher solid concentration, with a higher downward velocity close to the wall. This is evident as the specularity coefficient is decreased from 0.05 to 0, the latter corresponding to free-slip at the wall. Gas back mixing is clearly enhanced by solids downflow, and a high-upstream tracer concentration is predicted for low specularity coefficients. Once the specularity coefficient exceeds 0.05, it plays only a small role.

3-D Simulation with a low-specularity coefficient

Among various parameters examined in the sensitivity analyses, the specularity coefficient in the wall-boundary condition shows the greatest impact on predicted gas back mixing. It is expected that the wall effect should be more significant in 3-D columns than in 2-D systems. Benyahia et al.[54] suggested adjusting the specularity coefficient to fit the experimental data. However, this is unlikely to be feasible for large-scale fluidized beds with, only limited experimental data available.

Figures 14 to 16 compare predicted axial concentration profiles for ϕ = 0.05 and 0.005 with experimental data for three superficial gas velocities. A higher upstream tracer concentration is predicted for the low-specularity coefficient for all cases simulated, consistent with the 2-D parametric analyses. The low-specularity coefficient predictions show improved agreement with experimental data for U_g = 0.35 m/s. However, the upstream concentration profiles tend to be

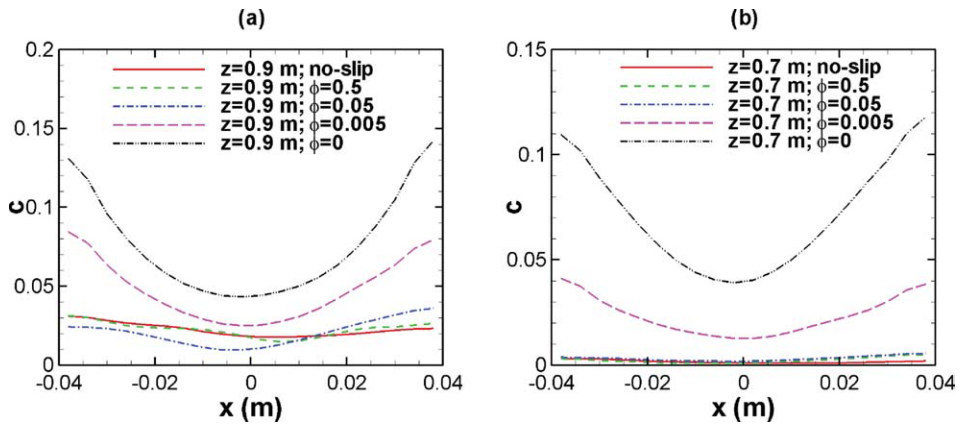

Figure 13. Effect of specularity coefficient on lateral profiles of upstream tracer concentration at (a) z = 0.9 m, (b) z = 0.7 m (U_g = 0.35 m/s, H_0 = 0.92 m, c_0 = 0.16, e_w = 0.8).

[Color figure can be viewed in the online issue, which is available at wileyonlinelibrary.com.]

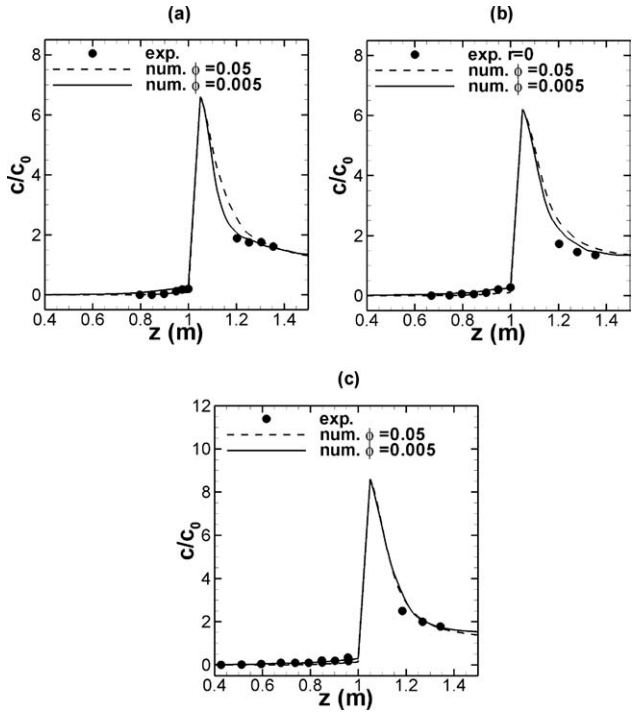

Figure 14. Axial profiles of mean tracer concentration at $r = 0$ for U_g = (a) 0.183 m/s, (b) 0.274 m/s, and (c) 0.354 m/s.

overpredicted for the other two gas velocities, especially for the lowest velocity of 0.18 m/s. This may suggest that the specularity coefficient is dependant on the superficial gas velocity, in addition to particle and wall properties.

The aforementioned analyses are confirmed by the radial profiles of tracer concentration shown in Figures 17 to 19. Downstream, as shown in Figure 17, no significant difference can be observed, except that the concentration profiles become slightly flatter, indicating improved radial mixing, as ϕ decreases from 0.05 to 0.005. Below the injection level, higher concentrations are predicted for low-specularity coefficient for all three cases. Figures 18 and 19 indicate that $\phi = 0.005$ gives good agreement with experimental data for $U_g = 0.35$ m/s, while a slightly higher specularity coefficient would give better agreement for the other two gas velocities. Again a lower superficial gas velocity requires a higher specularity coefficient. In-depth study is needed to clarify the relationship between specularity coefficient and superficial gas velocity, wall roughness and particle shape.

Back mixing

In fluidized-bed reactors, axial dispersion can significantly decrease conversion and product selectivity, and is, therefore, undesirable in most applications. It has been demonstrated in many studies[59–63] that gas back mixing is due to solids downflow, which drags gas downward when the velocity of descending particles exceeds the interstitial gas velocity. As shown previously, upstream tracer concentration near the wall is higher than in the central region of the column because solids downflow occurs predominantly close to the wall.

Mixing models are often used to characterize experimental data on gas mixing. Due to its simplicity, the most widely used model is the 1-D axial dispersion model (ADM).[2,64,65] In that case, based on an analogy with molecular diffusion, the axial dispersion coefficient quantifies gas mixing, lumping the combined effects of velocity fluctuations, nonuniform velocity profiles, and molecular diffusion into a single parameter, obtained by fitting experimental tracer data. The model may cause inaccurate predictions as it ignores radial gradients of concentration, voidage, and velocity,[66] disregards concentration differences between bubbles and dense phase,[12] and assume small-scale random mixing steps rather than large convective pulses or eddies.[7] For these reasons, 2-and 3-D dispersion models and multiphase models are often inaccurate. Moreover, they require solution of partial differential equations and need many inputs.

Thanks to CFD simulations, it is possible to obtain key information to study mixing in fluidized beds. As an alternative means to characterize back mixing, we define an instantaneous tracer backflow fraction B_{tracer}, the ratio of downward tracer flow through a cross section to the total tracer injection flow rate, i.e.

$$B_{tracer} = \frac{1}{2}\iint_A \alpha_g(|u_{g,z}| - u_{g,z})c_{\text{tracer}}ds/Q_{\text{tracer}} \qquad (5)$$

Similarly, an instantaneous gas backflow fraction $B_{g,z}$, can be defined as

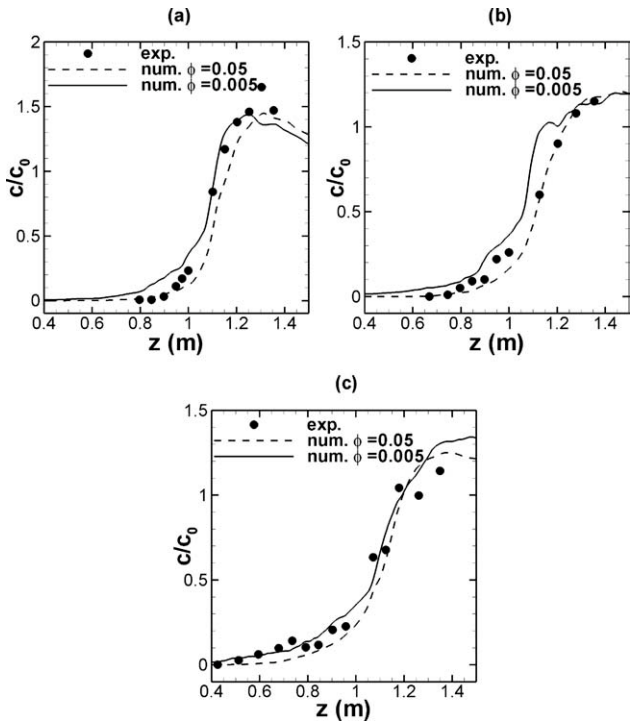

Figure 15. Axial profiles of mean tracer concentration at r = 28 mm for U_g = (a) 0.183 m/s, (b) 0.274 m/s, and (c) 0.354 m/s.

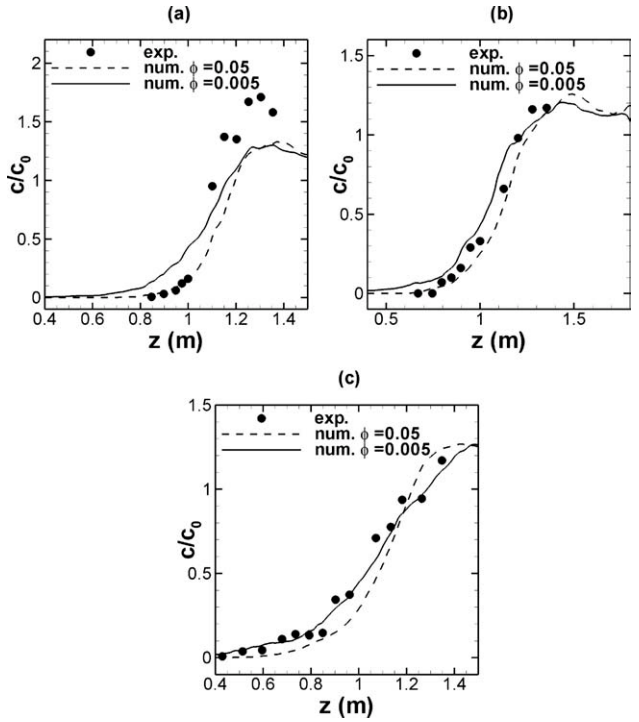

Figure 16. Axial profiles of mean tracer concentration at r = 36 mm for U_g = (a) 0.183 m/s, and (b) 0.274 m/s, and (c) 0.354 m/s.

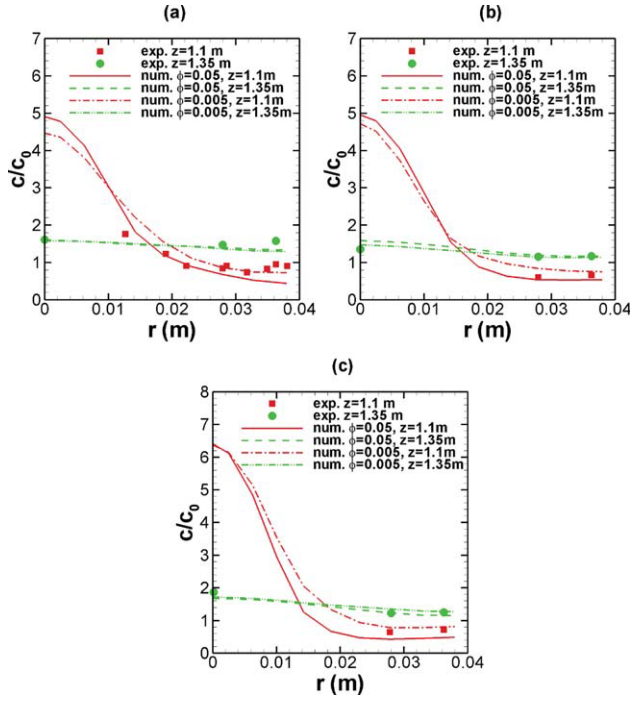

Figure 17. Radial profiles of mean tracer concentration above the injection level for U_g = (a) 0.183 m/s, (b) 0.274 m/s, and (c) 0.354 m/s.

[Color figure can be viewed in the online issue, which is available at wileyonlinelibrary.com.]

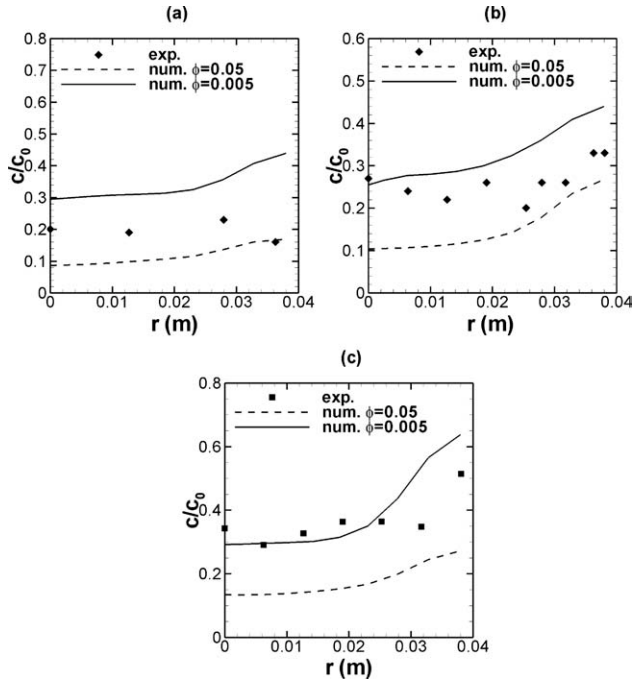

Figure 18. Radial profiles of mean tracer concentration at z = 1.0 m for U_g = (a) 0.183 m/s, (b) 0.274 m/s, and (c) 0.354 m/s.

$$B_{gas} = \frac{1}{2}\iint_A \alpha_g(|u_{g,z}| - u_{g,z})ds/Q_{\text{gas}} \tag{6}$$

where A indicates the cross section of the column, $u_{g,z}$ is the component of gas velocity in the flow direction. Q_{gas} and Q_{tracer} are the steady flow rates of fluidizing gas and tracer through the downstream cross section, respectively. With these two parameters, the gas back mixing is more accurately characterized than by axial dispersion models, which neglect the existence of two phases and their differences in volume fractions, gas velocities, and gas-flow rates, as well as being based on a deficient analogy.[7]

Figure 20 plots time-variations of tracer backflow fraction and gas backflow fraction upstream (z = 0.8 m) and downstream (z = 1.3 m) predicted by the 3-D numerical simulation. Intermittent gas and tracer backflow is predicted in both regions. The frequency of backflow is closely related to the slug frequency, as discussed later. There is significant backflow when a slug passes, with the peak magnitude of gas backflow fraction as high as two. It should be noted that the net gas flow through the cross section is still upward, although significant local instantaneous downward flow takes place. However, upstream, i.e., beneath the injection point, the time-averaged tracer gas flow through a cross section is zero by continuity. In the downstream region, profiles of B_{tracer} and B_{gas} are similar due to constant flow rate ratio of tracer gas and fluidizing gas and radial mixing of tracer with the fluidizing gas. However, in the upstream region, the backflow fraction of tracer is much smaller than that of the fluidizing gas, as only a small fraction of the tracer gas, injected on the axis of the column, is brought back and transported to that level. In addition, there are substantial

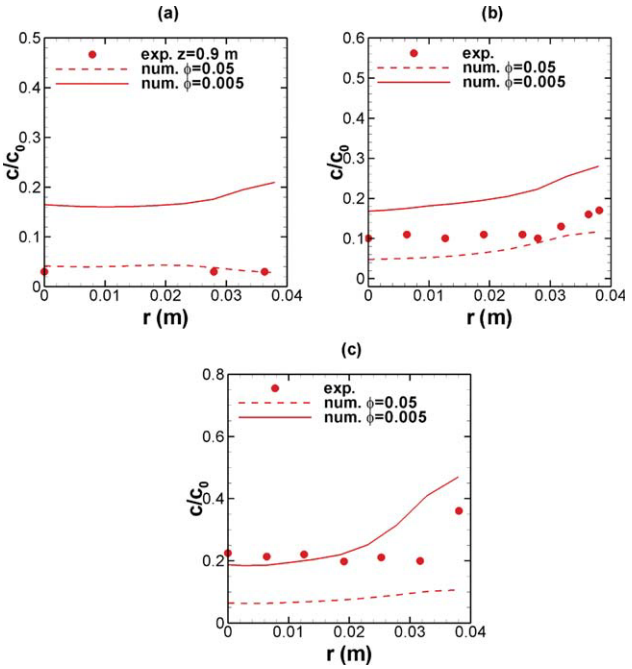

Figure 19. Radial profiles of mean tracer concentration at z = 0.9 m for U_g = (a) 0.183 m/s, (b) 0.274 m/s, and (c) 0.354 m/s.

[Color figure can be viewed in the online issue, which is available at wileyonlinelibrary.com.]

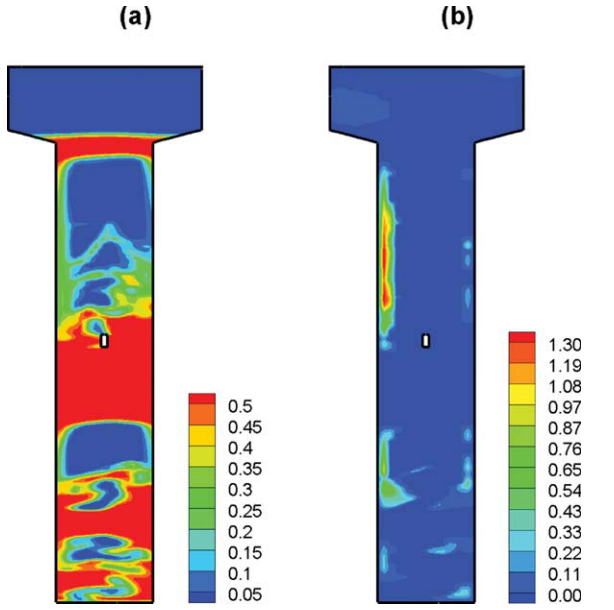

Figure 21. Contours of (a) solid-volume fraction, and (b) gas-back flux in a vertical symmetry plane at t = 43.7 s (U_g = 0.354 m/s, = 0.005, c_0 =11%).

[Color figure can be viewed in the online issue, which is available at wileyonlinelibrary.com.]

differences between the tracer and gas backflow fractions compared with those downstream, due to the unsteady variation of back mixing with time as a result of bubble/slug movement.

Figure 21 shows instantaneous contours of solid-volume fraction and gas-back flux, defined as $0.5\ \alpha_g(|u_{g,z}| - u_{g,z})$, in a vertical symmetry plane 43.7 s after start-up. There is a close relationship between the bubble/slug activities and the downward flow patterns, with backflow predominantly taking place close to the wall as slugs pass. It can be observed that tracer back mixing takes place due to radial gas mixing from the center injection port to the wall region, from where it is carried downward below the injection level. The back mixed tracer is then gradually extracted and carried upward by the upward gas flow. This is consistent with the mechanism

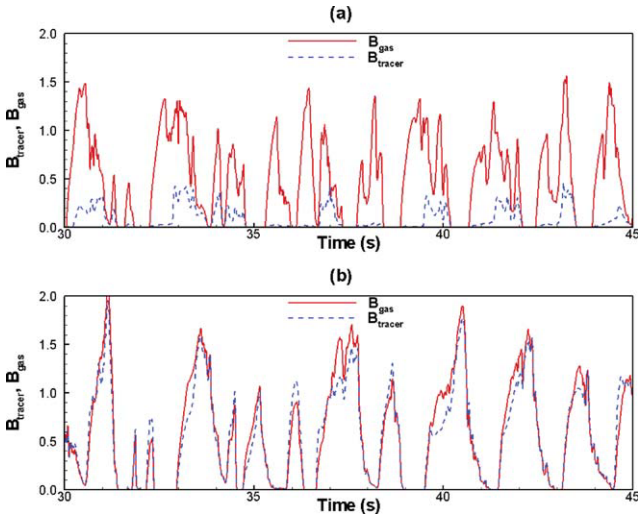

Figure 20. Tracer backflow fraction and gas backflow fraction vs. time across two planes; (a) z = 0.8 m, (b) z = 1.3 m (U_g = 0.354 m/s, ϕ = 0.005, c_0 = 11%).

[Color figure can be viewed in the online issue, which is available at wileyonlinelibrary.com.]

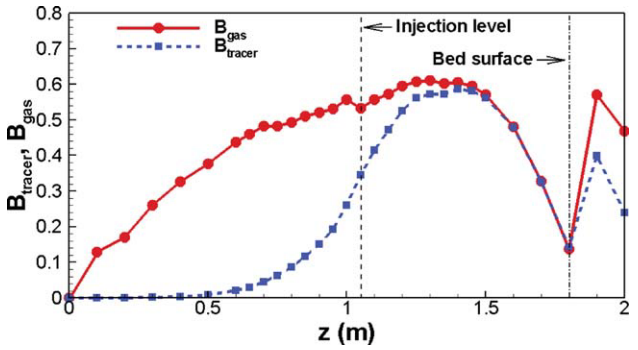

Figure 22. Time-averaged profiles of cross-sectional gas and tracer backflow rate profiles along the height of the column (U_g =0.354 m/s, = 0.005, c_0 = 11%; dashed vertical line: injection level; dashed-dot vertical line: bed surface).

[Color figure can be viewed in the online issue, which is available at wileyonlinelibrary.com.]

explained by van Deemter.[67] Hence, tracer back mixing is associated directly with gas and solids recirculation inside the system.

Mean gas and tracer backflow fractions at different heights predicted by the 3-D simulation are plotted in Figure 22. The gas backflow fraction is seen to increase gradually from zero at the distributor to a maximum in the upper region of the dense bed, then decreasing toward zero in the freeboard. Above the injection level, the profiles of tracer and gas backflow fractions become more and more similar. Below the injection level, the profile of tracer backflow fraction deviates clearly from the gas backflow fraction. The upstream tracer backflow fraction depends on both the gas backflow and the amount of tracer gas brought down to that level. The further upstream one looks, the smaller the concentration of tracer gas.

Gas back mixing was also investigated by examining the cross-sectional tracer concentration and the tracer and gas

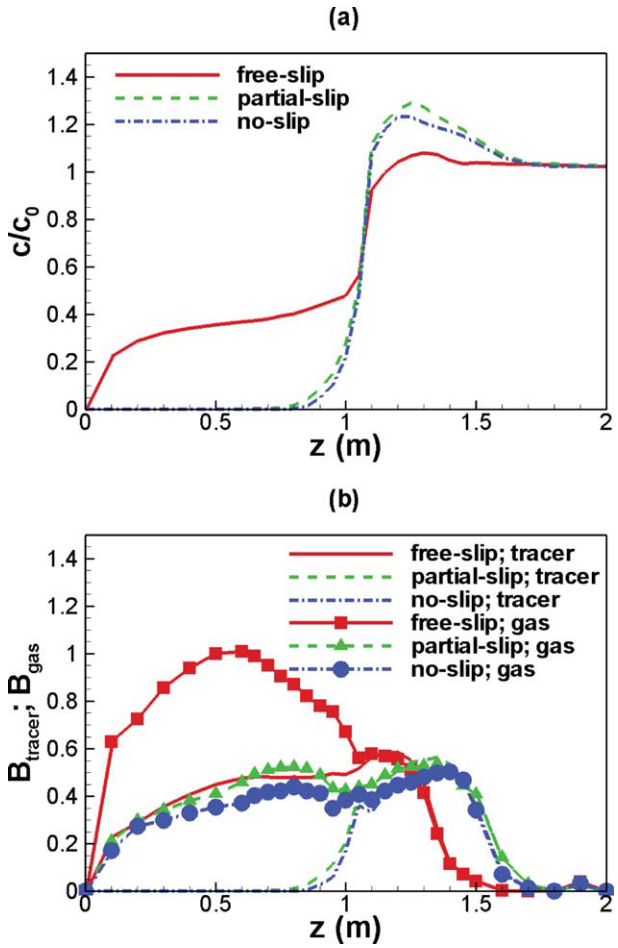

Figure 23. Influence of different wall boundary conditions on (a) cross-sectional averaged concentration, (b) tracer and gas backflow fraction profiles (U_g = 0.2 m/s, c_0 =0.1; line: tracer backflow fraction; line + symbol: gas backflow fraction).

[Color figure can be viewed in the online issue, which is available at wileyonlinelibrary.com.]

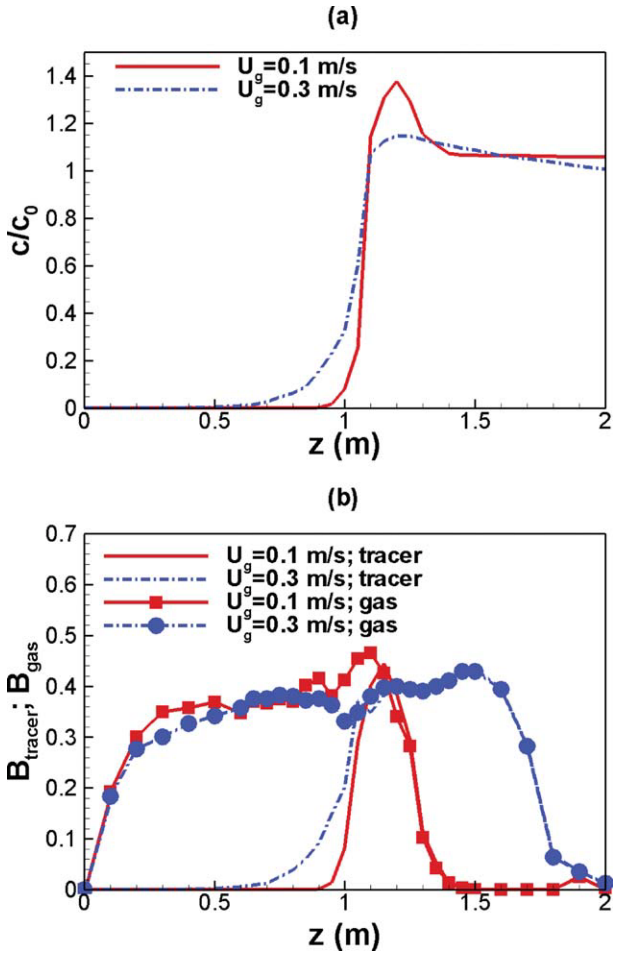

Figure 24. Influence of superficial gas velocity on axial profiles of (a) cross-section averaged tracer concentration, and (b) tracer and gas backflow fractions. (line: tracer backflow fraction; line + symbol: gas backflow fraction).

[Color figure can be viewed in the online issue, which is available at wileyonlinelibrary.com.]

backflow fractions predicted by 2-D simulations. The profiles of tracer and gas backflow fractions were almost identical when the transient numerical data were averaged over time intervals of 20, 30, and 50 s. Hence, in the remaining analyses, the profiles are averaged over 30 s for 2-D simulations and 20 s for 3-D simulations.

The influence of no-, partial- and free-slip wall boundary conditions on axial tracer concentration, tracer and gas backflow fractions is demonstrated in Figure 23. For the partial-slip boundary condition, a specularity coefficient of 0.05 is used. The particle-wall restitution coefficient was 0.8 in all cases. Except where otherwise noted, the axial tracer concentration profiles presented hereafter are cross-sectional averages of the numerical data. Profiles of tracer concentration, tracer and gas backflow fractions for the free-slip boundary condition differ considerably from those with partial- and no-slip wall conditions. Above the injection level, $c/c_0 > 1$ for all cases. It is also notable that the bed expansion

predicted with the free-slip wall condition is 15% lower than for the other two cases. Although it is not clear which wall-boundary condition is most appropriate, the free slip wall-boundary condition should be used only with caution. Note also that the results imply that both wall roughness and particle roughness (also shape) may significantly affect the extent of gas back mixing and the axial dispersion.

Results not shown here were also obtained for different tracer flow rates. The tracer back mixing decreased slightly as the injected pure tracer volumetric flow increased from 0.042 to 0.1 times the flow rate through the distributor. Profiles of axial tracer concentration, tracer and gas backflow fractions are shown in Figure 24 for superficial gas velocities of 0.1 and 0.3 m/s, with the tracer flow rate adjusted to maintain $c_0 = 0.1$. As the static bed height is constant, increased bed expansion with increasing gas velocity can be clearly observed. It can also be seen that the tracer backflow fraction increases with increasing superficial gas velocity. In an experimental slugging fluidized bed, gas back mixing has been reported to increase with increasing gas velocity and to go through a maximum near the transition to the turbulent fluidization regime.[4] As the gas velocities studied are below the transition velocity from slugging to turbulent fluidization, current numerical results are consistent with this experimental finding.

Conclusion

Three- and two-dimensional CFD simulations were performed for a fluidized bed in which detailed experimental measurements of gas mixing were reported in the literature. Detailed parametric studies were conducted, and the influence of several key parameters and assumptions were investigated. It was found that the solid-phase wall-boundary slip condition needs to be specified with great care when gas mixing is modeled, with free slip, partial slip and no-slip wall-boundary conditions giving substantial differences in the extent of gas downward transport at the wall. Axial and radial tracer concentration profiles are in reasonable agreement with the experimental data only if the specularity coefficient is chosen to give a good fit. CFD is a valuable tool for studying gas mixing in fluidized beds.

In this study, gas back mixing occurs due to intermittent downward motion of particles, especially those near the wall when gas slugs pass. Radial mixing of gas then transfers gas from the wall region to the interior of the region upstream of the trace injection level. Two new parameters, the tracer backflow fraction and the gas backflow fraction are introduced to assist in interpreting the axial dispersion results in numerical simulations. Qualitative trends are consistent with previous experimental findings.

Acknowledgments

The authors wish to acknowledge financial support from the Natural Sciences and Engineering Research Council (NSERC) of Canada.

Notation

A = cross-sectional area, m^2
B_{gas} = gas backflow fraction
B_{tracer} = tracer backflow fraction
$\overline{C}_{flux}$ = mean flux-based concentration, %
c = tracer concentration, mole fraction
c_0 = tracer concentration at exit, mole fraction
C_1, C_2 = model constants of $k - \varepsilon$ model
d_p = particle diameter, m
D = column diameter, m
D_m = gas molecular diffusivity, m^2/s
D_p = diffusion coefficient, m^2/s
e_p = coefficient of restitution for interparticle collisions
e_w = coefficient of restitution for particle-wall collisions
g = gravitational acceleration, m/s^2
G = production of turbulent kinetic energy, kg/m-s^3
H_0 = static bed height, m
H = expanded bed height, m
k = turbulent kinetic energy of gas phase, J/kg
k_{gp} = covariance of the velocities of gas phase and solid phase, J/kg
P = pressure, Pa
$P_{s,fric}$ = solid frictional pressure, Pa
$P_{s,vis}$ = solid pressure based on kinetic granular theory, Pa
Q_{gas} = gas-flow rate, m^3/s
Q_{tracer} = volumetric flow rate of tracer gas, m^3/s
r = radial distance, m
Sc = Schmidt number
t = time, s
U_g = superficial gas velocity, m/s
U_{mf} = minimum fluidization velocity, m/s
U_{ms} = minimum slugging velocity, m/s
$\vec{V}_g$ = velocity of gas phase, m/s
$\vec{V}_p$ = velocity of solid phase, m/s
$\vec{v}_{p,dr}$ = drift velocity of particle, m/s
Y_t = tracer-mass fraction
z = axial distance above distributor, m

Greek letters

α_g = gas-volume fraction
α_P = solid-volume fraction
$\alpha_{p,min}$ = solid-volume fraction to activate frictional model
$\alpha_{p,max}$ = maximum solid-volume fraction
β_{gp} = gas-solid drag coefficient, kg/m^3-s
ε = dissipation rate of gas-phase turbulent kinetic energy, m^2/s^3
ϕ = specularity coefficient
μ = gas viscosity, Pa-s
Θ_p = granular temperature, J/kg
ρ_g = fluidizing gas density, kg/m^3
ρ_p = particle density, kg/m^3
σ_k, σ_ε = model constants of $k - \varepsilon$ model
$\overline{\overline{\tau}}_p$ = solid-stress tensor, Pa
$\overline{\overline{\tau}}_{g,eff}$ = gas-stress tensor, Pa

Subscripts

back = backflow
g, gas = gas phase
p = particle/solid phase
tracer = tracer gas

Literature Cited

1. van Deemter JJ. *Mixing Patterns in Large-Scale Fluidized Beds*. In: Grace JR, Matsen JM, eds. *Fluidization*. New York: Plenum; 1980: 69–89.
2. Gilliland ER, Mason EA. Gas and solid mixing in fluidized beds. *Ind Eng Chem*. 1949;41:1191–1196.
3. Gilliland ER, Mason EA. Gas mixing in beds of fluidized solids. *Ind Eng Chem*. 1952;44:218–224.
4. Lee GS, Kim SD. Gas mixing in slugging and turbulent fluidized-beds. *Chem Eng Commun*. 1989;86:91–111.
5. Gayan P, deDiego LF, Adanez J. Radial gas mixing in a fast fluidized bed. *Powder Technol*. 1997;94:163–171.
6. Koksal M, Hamdullahpur F. Gas mixing in circulating fluidized beds with secondary air injection. *Chem Eng Res Des*. 2004;82:979–992.
7. Mireur JP, Bischoff KB. Mixing and contacting models for fluidized beds. *AIChE J*. 1967;13:839–845.

8. Atimtay A, Cakaloz T. Investigation on gas mixing in a fluidized-bed. *Powder Technol*. 1978;20:1–7.
9. Du B, Fan LS, Wei F, Warsito W. Gas and solids mixing in a turbulent fluidized bed. *AIChE J*. 2002;48:1896–1909.
10. Al-Sherehy F, Grace J, Adris AE. Gas mixing and modeling of secondary gas distribution in a bench-scale fluidized bed. *AIChE J*. 2004;50:922–936.
11. Song XQ, Grace JR, Bi H, Lim CJ, Chan E, Knapper B, McKnight CA. Gas mixing in the reactor section of fluid cokers. *Ind Eng Chem Res*. 2005;44:6067–6074.
12. Davidson JF, Clift R, Harrison D. *Fluidization*. Orlando: Academic Press; 1985.
13. Kunii Do, Levenspiel O. *Fluidization Engineering*. New York: Wiley; 1969.
14. Davidson JF, Harrison D. *Fluidization*. New York: Academic Press; 1971.
15. Patil DJ, Annaland MS, Kuipers JAM. Gas dispersion and bubble-to-emulsion phase mass exchange in a gas-solid bubbling fluidized bed: a computational and experimental study. *Int J Chem Reactor Eng*. 2003;A44:1.
16. Li T, Pougatch K, Salcudean M, Grecov D. Mixing of secondary gas injection in bubbling fluidized beds. *Chem Eng Res Des*. 2009;87:1451–1465.
17. Mason EA. *Gas mixing in Beds of Fluidized Solids*. Massachusetts Institute of Technology: Massachusetts; 1950.
18. Gidaspow D. *Multiphase Flow and Fluidization: Continuum and Kinetic Theory Descriptions*. Boston: Academic Press; 1994.
19. Lun CKK, Savage SB, Jeffrey DJ, Chepurniy N. Kinetic theories for granular flow - inelastic particles in Couette flow and slightly inelastic particles in a general flow field. *J Fluid Mech*. 1984;140:223–256.
20. Fluent. *FLUENT 6.3 documentation*. Fluent, Inc; 2006.
21. Andrews AT, Loezos PN, Sundaresan S. Coarse-grid simulation of gas-particle flows in vertical risers. *Ind Eng Chem Res*. 2005; 44:6022–6037.
22. Busciglio A, Vella G, Micale G, Rizzuti L. Analysis of the bubbling behavior of 2D gas solid fluidized beds Part II. Comparison between experiments and numerical simulations via digital image analysis technique. *Chem Eng J*. 2009;148:145–163.
23. Zhang DZ, Vander Heyden WB. High-resolution three-dimensional numerical simulation of a circulating fluidized bed. *Powder Technol*. 2001;116:133–141.
24. Johnson PC, Jackson R. Frictional collisional constitutive relations for antigranulocytes-materials, with application to plane shearing. *J Fluid Mech*. 1987;176:67–93.
25. Stewart PSB, Davidson JF. Slug flow in fluidised beds. *Powder Technol*. 1967;1:61–80.
26. Wen CY, Yu YH. A generalized method for predicting minimum fluidization velocity. *AIChE J*. 1966;12:610–612.
27. Yang TY, Leu LP. Study of transition velocities from bubbling to turbulent fluidization by statistic and wavelet multi-resolution analysis on absolute pressure fluctuations. *Chem Eng Sci*. 2008;63:1950–1970.
28. Johansson K, van Wachem BGM, Almstedt AE. Experimental validation of CFD models for fluidized beds: Influence of particle stress models, gas phase compressibility and air inflow models. *Chem Eng Sci*. 2006;61:1705–1717.
29. McKeen T, Pugsley T. Simulation and experimental validation of a freely bubbling bed of FCC catalyst. *Powder Technol*. 2003;129: 139–152.
30. van Wachem BGM, Schouten JC, Krishna R, van den Bleek CM. Validation of the Eulerian simulated dynamic behaviour of gas-solid fluidised beds. *Chem Eng Sci*. 1999;54:2141–2149.
31. Pain CC, Mansoorzadeh S, Gomes JLM, de Oliveira CRE. A numerical investigation of bubbling gas-solid fluidized bed dynamics in 2-D geometries. *Powder Technol*. 2002;128:56–77.
32. Hulme I, Clavelle E, van der Lee L, Kantzas A. CFD modeling and validation of bubble properties for a bubbling fluidized bed. *Ind Eng Chem Res*. 2005;44:4254–4266.
33. Zimmermann S, Taghipour F. CFD modeling of the hydrodynamics and reaction kinetics of FCC fluidized-bed reactors. *Ind Eng Chem Res*. 2005;44:9818–9827.
34. Geldart D. The size and frequency of bubbles in two-and three-dimensional gas-fluidized beds. *Powder Technol*. 1970;4:41–55.
35. Peirano E, Delloume V, Leckner B. Two- or three-dimensional simulations of turbulent gas-solid flows applied to fluidization. *Chem Eng Sci*. 2001;56:4787–4799.
36. Cammarata L, Lettieri P, Micale GDM, Colman D. 2D and 3D CFD simulations of bubbling fluidized beds using Eulerian-Eulerian models. *Int J Chem Reactor Eng*. 2003;A48:1.
37. Xie N, Battaglia F, Pannala S. Effects of using two- versus three-dimensional computational modeling of fluidized beds—Part I, hydrodynamics. *Powder Technol*. 2008;182:1–13.
38. Xie N, Battaglia F, Pannala S. Effects of using two- versus three-dimensional computational modeling of fluidized beds: Part II, budget analysis. *Powder Technol*. 2008;182:14–24.
39. Foerster SF, Louge MY, Chang AH, Allia K. Measurements of the collision properties of small spheres. *Phys Fluids*. 1994;6:1108–1115.
40. Lun CKK, Savage SB. The effects of an impact velocity dependent coefficient of restitution on stresses developed by sheared granular materials. *Acta Mechanica*. 1986;63:15–44.
41. Samuelsberg A, Hjertager BH. An experimental and numerical study of flow patterns in a circulating fluidized bed reactor. *Int J Multiphase Flow*. 1996;22:575–591.
42. Goldschmidt MJV, Kuipers JAM, van Swaaij WPM. Hydrodynamic modeling of dense gas-fluidised beds using the kinetic theory of granular flow: effect of coefficient of restitution on bed dynamics. *Chem Eng Sci*. 2001;56:571–578.
43. Lu HL, He YR, Liu WT, Ding JM, Gidaspow D, Bouillard J. Computer simulations of gas-solid flow in spouted beds using kinetic-frictional stress model of granular flow. *Chem Eng Sci*. 2004;59: 865–878.
44. Du W, Bao XJ, Xu J, Wei WS. Computational fluid dynamics (CFD) modeling of spouted bed: Influence of frictional stress, maximum packing limit and coefficient of restitution of particles. *Chem Eng Sci*. 2006;61:4558–4570.
45. Taghipour F, Ellis N, Wong C. Experimental and computational study of gas-solid fluidized bed hydrodynamics. *Chem Eng Sci*. 2005;60:6857–6867.
46. Reuge N, Cadoret L, Coufort-Saudejaud C, Pannala S, Syamlal M, Caussat B. Multifluid Eulerian modeling of dense gas-solids fluidized bed hydrodynamics: Influence of the dissipation parameters. *Chem Eng Sci*. 2008;63:5540–5551.
47. Li T, Pougatch K, Salcudean M, Grecov D. Numerical simulation of a spouted bed with a draft tube with and without liquid spray. *Can J Chem Eng*. 2009;87:237–251.
48. Crowe CT, Troutt TR, Chung JN. Numerical models for two-phase turbulent flows. *Annu Rev Fluid Mech*. 1996;28:11–43.
49. Enwald H, Peirano E, Almstedt AE. Eulerian two-phase flow theory applied to fluidization. *Int J Multiphase Flow*. 1996;22:21–66.
50. Portela LM, Oliemans RVA. Possibilities and limitations of computer simulations of industrial turbulent dispersed multiphase flows. *Flow Turbu Combust*. 2006;77:381–403.
51. Lindborg H, Lysberg M, Jakobsen HA. Practical validation of the two-fluid model applied to dense gas-solid flows in fluidized beds. *Chem Eng Sci*. 2007;62:5854–5869.
52. Benyahia S. Gas/Solids turbulence models implemented in MFIX. 2005.
53. Natarajan VVR, Hunt ML. Kinetic theory analysis of heat transfer in granular flows. *Int J Heat Mass Transfer*. 1998;41:1929–1944.
54. Benyahia S, Syamlal M, O'Brien TJ. Study of the ability of multiphase continuum models to predict core-annulus flow. *AIChE J*. 2007;53:2549–2568.
55. Zhang YH, Reese JM. Gas turbulence modulation in a two-fluid model for gas-solid flows. *AIChE J*. 2003;49:3048–3065.
56. Zhang SJ, Yu AB. Computational investigation of slugging behaviour in gas-fluidised beds. *Powder Technol*. 2002;123:147–165.
57. Neri A, Gidaspow D. Riser hydrodynamics: Simulation using kinetic theory. *AIChE J*. 2000;46:52–67.
58. Almuttahar A, Taghipour F. Computational fluid dynamics of high density circulating fluidized bed riser: study of modeling parameters. *Powder Technol*. 2008;185:11–23.
59. Stephens GK, Sinclair RJ, Potter OE. Gas exchange between bubbles and dense phase in a fluidized bed. *Powder Technol*. 1967;1:157.
60. Nguyen HV, Whitehead AB, Potter OE. Gas backmixing, solids movement, and bubble activities in large-scale fluidized-beds. *AIChE J*. 1977;23:913–922.

61. Nguyen HV, Potter OE, Dent DC, Whitehead AB. Gas backmixing in large fluidized-beds containing tube assemblies. *AIChE J*. 1981;27:509–514.
62. Li JH, Weinstein H. An experimental comparison of gas backmixing in fluidized-eeds across the regime spectrum. *Chem Eng Sci*. 1989;44:1697–1705.
63. Deshmukh SARK, Annaland MV, Kuipers JAM. Gas back-mixing studies in membrane assisted bubbling fluidized beds. *Chem Eng Sci*. 2007;62:4095–4111.
64. Cho HI, Chung CH, Han GY, Ahn GR, Kong JS. Axial gas dispersion in a fluidized bed of polyethylene particles. *Korean J Chem Eng*. 2000;17:292–298.
65. Zhang YM, Lu CX, Grace JR, Bi XT, Shi M. Gas back-mixing in a two-dimensional baffled turbulent fluidized bed. *Ind Eng Chem Res*. 2008;47:8484–8491.
66. Grace J, Bi H, Zhang Y. Pitfalls in gas sampling from fluidized beds. *Chem Eng Sci*. 2009;64:2522–2524.
67. van Deemter JJ. Mixing and contacting in gas solid fluidized beds. *Chem Eng Sci*. 1961;13:143–154.

Manuscript received July 27, 2009, revision received Sept. 20, 2009, and final revision received Nov. 24, 2009.